buildings

MDPI

Article

Rheological Properties and Permeation Grouting Reinforcement Effect of Cement-Bentonite Slurry

Yuan Wang [1], Tian Qi [2], Chenxi Xu [2,*] and Jiakun Gong [2,*]

[1] College of Water Conservancy and Hydropower Engineering, Hohai University, Nanjing 210098, China
[2] College of Mechanics and Engineering Science, Hohai University, Nanjing 211100, China
* Correspondence: 221308010036@hhu.edu.cn (C.X.); jiakungong@hhu.edu.cn (J.G.)

Abstract: Permeation grouting is one important method for preventing and controlling leakage in levees, with cement-bentonite slurry as a commonly used grouting material. In this study, the effect of water–cement ratio and bentonite content on the rheological properties of cement-bentonite slurry was investigated. The reinforcement effect of cement-bentonite slurry under various conditions was explored by conducting a series of experiments via a self-designed apparatus. The grouting pressure, water–cement ratio, and bentonite content were taken as the grouting variables, and the compressive strength, deformation modulus, and permeability coefficient were adopted as indicators to evaluate the reinforcement effect. The experimental results indicate that the plastic viscosity and the yield stress of the cement-bentonite slurry rose as the water–cement ratio increased. The water–cement ratio served as the main controlling factor of the grouting reinforcement effect. The compressive strength, deformation modulus, and permeability of the grouted body decreased as the water–cement ratio increased. The bentonite content significantly impacted the grouting reinforcement effect. As the bentonite content of slurry increased, the permeability of the grouted body increased, while the compressive strength and deformation modulus first increased then decreased. An optimal bentonite content of cement-bentonite slurry can be decided. Moreover, the failure mode of the grouted body was also significantly impacted by the water–cement ratio. As the water–cement ratio increased, the heterogeneity of the grouted body became greater, and the failure mode changed from overall failure to local failure. The heterogeneity of the grouted body can be improved by enhancing the grouting pressure and the bentonite content of cement-bentonite slurry.

Keywords: permeation grouting; cement-bentonite slurry; rheological properties; grouting reinforcement effect

check for updates

Academic Editors: Salvatore Verre, Grzegorz Ludwik Golewski, Wei Sun, Yu Tian and Ran Yuan

Received: 28 December 2024
Revised: 5 February 2025
Accepted: 18 February 2025
Published: 25 February 2025

Citation: Wang, Y.; Qi, T.; Xu, C.; Gong, J. Rheological Properties and Permeation Grouting Reinforcement Effect of Cement-Bentonite Slurry. *Buildings* **2025**, *15*, 744. https://doi.org/10.3390/buildings15050744

Copyright: © 2025 by the authors. Licensee MDPI, Basel, Switzerland. This article is an open access article distributed under the terms and conditions of the Creative Commons Attribution (CC BY) license (https://creativecommons.org/licenses/by/4.0/).

1. Introduction

Floods are a serious challenge in China, and numerous flood hazards have occurred in history. Global warming further exacerbates the frequency of extreme rainfall, thereby intensifying the destructiveness of flood hazards. Over the centuries, China has developed a series of dike systems, such as the Yangtze River Dike and the Hongze Lake Dike, which form the core of flood control and disaster mitigation system in China. However, the dikes are primarily constructed using local materials, such as sand, gravel, and clay. A significant portion of the dikes have undergone multiple heightening and reinforcement phases in history, resulting in highly heterogeneous foundations. The presence of cracks, cavities, and loose bodies makes the dikes particularly susceptible to piping and other types of seepage damage during flood seasons [1,2]. Grouting is a crucial method for managing seepage-related dike disasters [3]. Permeation grouting, in particular, is widely used in dike

engineering due to its minimal disturbance to the injected medium during the grouting process, and the excellent application results [4].

Common grouting materials include chemical grout and cement-based grout. Chemical grout offers advantages such as low viscosity, controllable gelation time, and the ability to penetrate in fine cracks, while disadvantages are in the aspects of economy, durability, and environmental protection [5]. Cement-based grout is widely applied due to its environmental friendliness, low cost, and great impermeability [6,7]. However, traditional cement grout suffers from severe bleeding and instability during the grouting process. Bentonite can effectively alleviate slurry bleeding, enhancing its stability, pumpability, and impermeability [8]. Extensive research has been conducted on bentonite-modified cement grout. Mirza et al. [9] investigated the reactivity of bentonite in mortar and concrete, assessing the optimal substitution level for durability. Jiang et al. [10] studied the effects of bentonite type, dosage, and water–cement ratio on the workability and permeability coefficient of bentonite cement mortar. Li [11] explored the possibility of improving the filling material's contact ratio and volume stability by applying the expansiveness of bentonite. Xu et al. [12] examined the impact of bentonite dosage on the bleeding characteristics of cement slurry. Todaro et al. [13] investigated the effects of activation time of bentonite on the bleeding and compressive strength of grouting materials. Regarding the strength of solidified cement-bentonite slurry, different conclusions have been reached. Zhang et al. [14] and Zhao et al. [15] found that bentonite inhibits the hydration reactions and plastifies hardened materials, thereby reducing the compressive strength. On the contrary, Wang et al. [16] and Li [11] discovered that the inclusion of bentonite enhances the compressive strength of solidified slurry due to its particlefilling effect, which improves material strength [17]. In the study of permeable grouting using cement-bentonite slurry as the grouting material, Santhoshkumar et al. [18] conducted experimental research on the influence of bentonite on the flow of cement grout in coarse sandy soil, finding that bentonite can enhance the lateral diffusion of the grout. Qing et al. [19] investigated the applicability of cement-bentonite slurry for permeable grouting in gravelly soil, discovering that the incorporation of bentonite into the slurry reduced the diffusion distance of the grout while slightly enhancing the strength of the grouted body. Cheng et al. [20] selected a cement-bentonite slurry with the minimum bleeding rate through bleeding tests and conducted a series of water injection and grouting experiments to study the threshold seepage velocity, initiation pressure, and factors influencing the initiation pressure. Zhang [21] conducted theoretical analysis on the flow mechanisms of cement-bentonite slurry in fractures and investigated the flow capacity of cement-bentonite slurry in combination with laboratory tests. Cheng [22] added bentonite to ordinary cement for permeable grouting, effectively addressing the issue of filling effectiveness in microfractures.

In summary, the current research on cement-bentonite slurry primarily focuses on the improvement of slurry properties such as workability and bleeding. However, there is a lack of study on the time-varying properties of cement-bentonite slurry during permeation grouting and the mechanisms by which key grouting parameters, such as bentonite dosage, affect the properties of grouted body. This gap in knowledge makes it challenging to provide reliable support for grouting projects.

In this study, we first investigated the mechanisms of the water–cement ratio and bentonite dosage affecting the rheological properties of cement-bentonite slurry. The impacts of water–cement ratio, grouting pressure, and bentonite dosage on grouting quality were explored through a series of orthogonal experiments. The compressive strength, deformation modulus, and permeability coefficient were adopted as the evaluation indices for the effectiveness of permeation grouting reinforcement to study.

2. Materials and Methods

2.1. Experimental Apparatus

2.1.1. Apparatus for Rheological Properties of Cement-Bentonite Slurry

The rheological properties of the slurry were measured using an RST-SST rheometer. This rheometer enables the analysis of yield stress and viscosity performance; it employs a paddle rotor and offers two control modes: shear stress and shear rate. Prior to rheological measurements, the slurry was mixed using a JJ-5 cement mortar mixer. The mixer has two speed settings for the mixing blades: low speed and high speed. At low speed, the blade rotation rate is 140 ± 5 rpm (revolutions per minute), and the planetary rotation rate is 62 ± 5 rpm. At high speed, the blade rotation rate is 285 ± 10 rpm, and the planetary rotation rate is 125 ± 10 rpm.

2.1.2. Apparatus for Cement-Bentonite Slurry Permeation Grouting

The permeation grouting apparatus consists of five parts: an air compressor, a pressure stabilizer, a slurry storage tank, and the injected medium. During the experiment, air was injected into the slurry storage tank through the pressure stabilizer by the air compressor, which provided driving force to push the slurry into the specimen (Figures 1 and 2). The grouting pressure remained constant throughout the injection process.

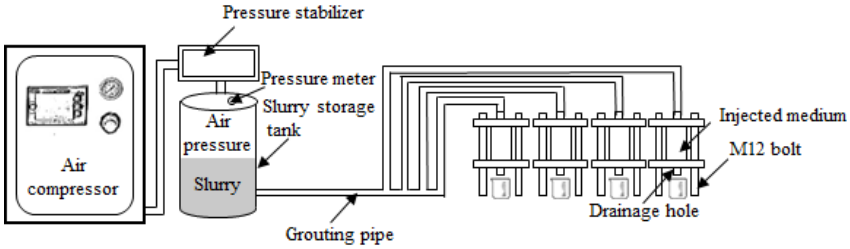

Figure 1. Schematic of permeation grouting apparatus.



Figure 2. Permeation grouting experimental apparatus.

The air compressor can provide air pressure ranging from 0 to 1.0 MPa. The pressure stabilizer maintained the air pressure at a set value to ensure constant-pressure grouting conditions. The slurry storage tank had dimensions of Φ160 mm × 300 mm, with a wall thickness of 10 mm. The top cover is removable for slurry filling and cleaning. A pressure gauge was installed on the top cover to monitor the grouting pressure inside the tank. The top cover and the tank body were sealed with a silicone gasket and secured with bolts.

Prior to the experiment, a bentonite suspension was prepared and allowed to stand for 24 h. Subsequently, cement meeting the water–cement ratio requirements was incorporated, and the mixture was thoroughly agitated for 5 min using a mixer. This mixer features a rotational speed ranging from 0 to 850 revolutions per minute (r/min) with 1 to 6 speed

settings, enabling precise control over the mixing rate (Figure 3). During the experiment, the slurry was first filled into the storage tank. Air was then injected from the top of the tank, and the slurry flowed out from the outlet (bottom) through grouting pipes into the injected medium. The apparatus was equipped with four grouting pipes, each with an inner diameter of 15 mm, allowing the slurry to be simultaneously injected into four models, which effectively improves grouting efficiency.

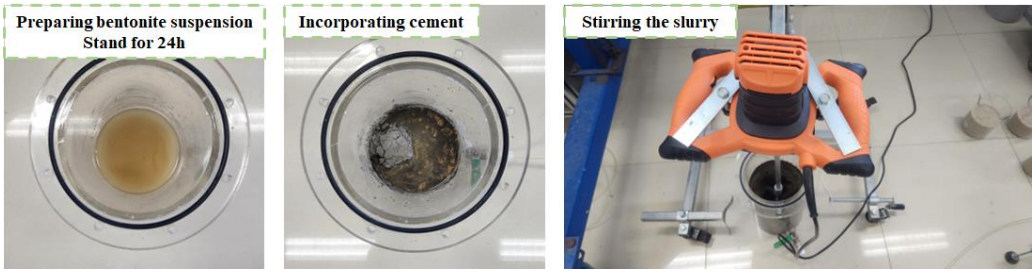

Figure 3. Preparation of cement-bentonite slurry.

The grouting medium model was made of iron-carbon alloy (Figure 4). The central pressure-bearing tube had dimensions of Φ50 mm × 110 mm with a wall thickness of 10 mm. The top cover and bottom plate were each 10 mm thick, and they were tightened with M12 bolts, which were long enough to serve as supporting legs. Silicone gaskets were placed between the top cover, bottom plate, and the sample holder to ensure the apparatus was sealed. The sample holder was filled with a sand sample to be grouted, with a filter screen placed on top to prevent structural damage to the sample. A 10 cm thick permeable stone layer was placed at the bottom of the sand sample to prevent structural damage and allow water to flow out.

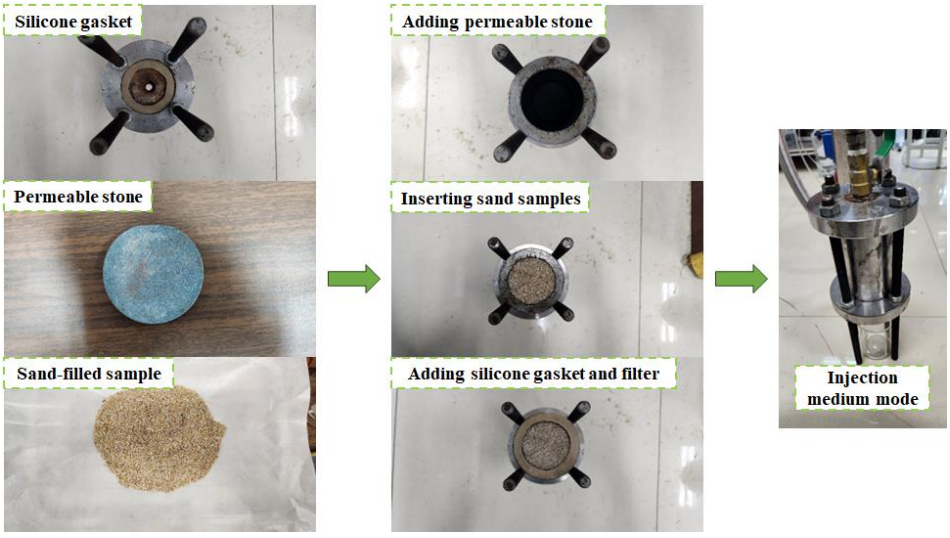

Figure 4. Injection medium model.

The grouting time was 2 min. Once the grouting process was completed, the entire sample holder was placed into a curing chamber, where the temperature was maintained at 20 °C and the humidity was kept at 95% for 3 days.

2.1.3. Apparatus for Cement-Bentonite Slurry Grouting Reinforcement Performance Uniaxial Compression Test Apparatus

Once the grouting model reached the specified curing time, it was demolded using an electric hydraulic demolder. Subsequently, the uniaxial compressive strength and

deformation modulus of the reinforced specimen were measured using a universal testing machine (UTM). The UTM was programmed to apply a loading force at a rate of 1 kN/s and record the maximum load sustained by the specimen along with the corresponding axial displacement.

In this segment of the experimentation, the compressive strength of the grout-reinforced solid was ascertained based on the maximum pressure sustained by the specimen. The modulus of deformation, on the other hand, was determined by both the maximum pressure endured by the specimen and the corresponding strain value at this peak pressure.

Permeability Coefficient Test Apparatus

In conventional permeability coefficient tests, the specimen is typically demolded and placed into the test apparatus, leading to unavoidable gaps between the specimen and the apparatus walls. These gaps can result in inaccurately high permeability coefficient measurements. To address this issue, the following method was adopted in this study: after curing, the grouted sample was not demolded; instead, the same apparatus was used to measure the permeability coefficient directly. The permeability coefficient test apparatus was composed of several key components: an air compressor, a pressure stabilizer, a water storage tank, a sample holder, and a beaker (Figure 5).

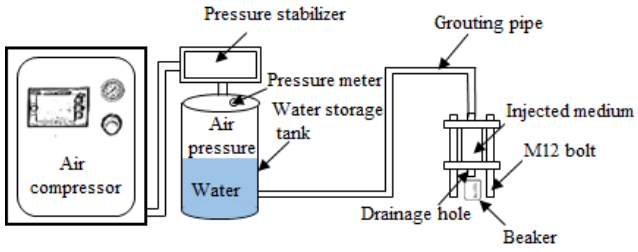

Figure 5. Schematic of the permeability coefficient test apparatus.

The permeability coefficient of the grouted specimen was determined through constant-head tests. Water was injected into the specimen through the injection hole on top of the sample holder under constant pressure and flowed out through the drainage outlet at the bottom. The volume of water discharged was measured using a beaker over a specified time period under defined pressure conditions. The permeability coefficient of the specimen was then calculated using Equation (1) [23].

$$K = \frac{\rho g Q}{AT} \frac{L}{\Delta p} \quad (1)$$

where K is the permeability coefficient of the grouted body; ρ is the density of water, ρ = 1000 kg/m^2; g is the acceleration due to gravity, g = 9.8 m/s^2; A is the cross-sectional area of the specimen, A = 19.63 cm^2; T is time, s; Q is the volume of water discharged during time T, cm^3; L is the length of the flow path through the specimen, L = 10 cm; and Δp is the pressure difference across the specimen, Δp = 0.5 Mpa.

The permeability coefficients of samples cured for 6 h, 12 h, and 24 h were measured. It was observed that for the 6 h cured samples, water started to flow out from the bottom within 30 s of injection. For these samples, the measurement time T was set to 120 s, and the test was repeated five times to obtain an average value. For the 12 h cured samples, water started to flow out within 120 s of injection. The measurement time T was set to 300 s, with the test repeated five times to obtain an average value. For the 24 h cured samples, nearly no water flowed out within 30 min of injection, making it difficult to accurately measure the water volume Q. Therefore, the permeability coefficients of the 6 h and 12 h cured samples were used as indicators for evaluating the impermeability of the specimens.

2.2. Experimental Method

2.2.1. Experimental Variables

In this study, the water–cement ratio and bentonite content were used as variables in the preparation of slurry to study the rheological properties of different slurries. The grouting pressure, water–cement ratio, and bentonite content were adopted as variables in the permeation grouting experiments, with compressive strength, deformation modulus, and permeability coefficient serving as indicators to evaluate the effectiveness of the permeation grouting on the specimens.

According to Wang's study [24] on the injectivity of sandy layers, a sand sample with particle size range of 1~2 mm was applied as the injected medium, which was in a dry condition initially. Before the experiment, the sand was washed and dried. The specific gravity of the sample was determined according to the "Standard for Soil Test Methods" [25]. The required mass of the injected medium was calculated based on the set porosity, while the permeability coefficient was measured through the constant head permeability test. The main parameters of the injected medium are shown in Table 1.

Table 1. Main parameters of the injected medium.

Parameter	Specific Gravity (-)	Particle Size Range (mm)	Porosity (-)	Permeability Coefficient (cm/s)
Numerical value	2.65	1~2	0.394	2.54×10^{-1}

Based on the research presented in literature [26], splitting occurs when the grouting pressure exceeds 1 MPa. To avoid the occurrence of splitting during the grouting process in the experiments, and considering the pressure range supplied by the air compressor, three levels of grouting pressure were determined: 0.2 MPa, 0.4 MPa, and 0.6 MPa.

The cement material used in the experiment was P.O 42.5 ordinary Portland cement from Zhucheng Jiuqi Building Materials Co., Ltd. (Weifang, China). The cement had an initial setting time greater than 150 min and a final setting time less than 240 min. Its 3-day flexural strength exceeded 5.5 MPa, and its 3-day compressive strength exceeded 27.5 MPa. Furthermore, the 28-day flexural strength was greater than 8.0 MPa, and the 28-day compressive strength was greater than 49.0 MPa. The detailed chemical composition of the cement material was obtained directly from the manufacturer and is presented in Table 2. In seepage prevention and reinforcement projects of dikes, the commonly utilized water–cement ratio for cement grout is 1.00. To investigate the influence of the water–cement ratio on the process of permeable grouting, the experiments were designed with grout water–cement ratios set at 0.80, 1.00, and 1.25.

Table 2. Chemical composition of Portland cement P.O 42.5.

Chemical Composition	SiO_2	Al_2O_3	Fe_2O_3	CaO	MgO	SO_3	CL^-	LOI
Mass percentage (%)	24.99	8.26	4.03	51.42	3.71	2.51	0.04	3.31

The bentonite used in the experiments was sodium bentonite sourced from Nanjing Tangshan Bentonite Co., Ltd. (Nanjing, China). Prior to the experiments, the bentonite was sieved using a 200-mesh standard sieve (0.075 mm) to prevent any internal impurities within the bentonite from affecting the test results. Its physical properties and chemical composition are detailed in Tables 3 and 4, respectively.

Table 3. Physical properties of sodium-based bentonite.

Type	200-Mesh Pass Rate (%)	Gelatinous Value (mL/g)	Swelling Capacity (mL/g)	Montmorillonite Content (%)	Water Absorption Capacity (%)
Sodium-based bentonite	95	1500	64	90	200

Table 4. Chemical composition of sodium-based bentonite.

Chemical Composition	SiO_2	Al_2O_3	Fe_2O_3	CaO	MgO	Na_2O
Mass percentage (%)	71.43	19.76	2.03	0.76	2.28	1.50

The encapsulating effect and porous microstructure of bentonite are detrimental to hydration reactions and strength development. Therefore, the bentonite content should not exceed 5% [27]. Three levels of bentonite content were set at 1%, 3%, and 5% (mass relative to the water), with a control group of 0% bentonite, i.e., pure cement slurry.

2.2.2. Experimental Design

Slurry Rheological Property Test

In the test of rheological property, bentonite suspension with specified bentonite content was prepared and stood for 24 h to ensure stability. Cement was then added to the suspension to achieve the predetermined water–cement ratio, and the mixture was stirred for 2 min afterwards. The rheological properties of the slurry were then evaluated using a BROOKFIELD RST-SST rheometer. The shear rate was programmed to increase from 0 to 100 s^{-1} over a period of 15 s. The shear stress was recorded at various shear rates after different resting times, i.e., 0, 15, 30, 45, and 60 min. The rheological curves can then be plotted.

Grouting Reinforcement Test

The grouting reinforcement test design involved 3 factors, with a maximum of 4 levels for each factor. An L16(4^3) orthogonal array was selected, and the factor level table is shown in Table 5.

Table 5. Factor level table.

Levels	Factors		
	Grouting Pressure (MPa)	Water–Cement Ratio (-)	Bentonite Content (%)
1	0.2	0.80	0
2	0.4	1.00	1
3	0.6	1.25	3
4	-	-	5

Considering that the number of levels for each factor differs, the experimental design was improved using the "desired level method" [28]. The improved experimental scheme and results are presented in Table 6.

Table 6. Test designs and test results.

Sample Numbers	Factor 1 Grouting Pressure (MPa)	Factor 2 Water–Cement Ratio (-)	Factor 3 Bentonite Content (%)	Post-Grouting Test Results			
				3-Day Compressive Strength (MPa)	3-Day Deformation Modulus (MPa)	6 h Permeability Coefficient (cm/s)	12 h Permeability Coefficient (cm/s)
1	0.2	0.80	0	5.72	390.44	7.038×10^{-6}	1.877×10^{-6}
2	0.2	1.00	1	2.96	242.80	1.023×10^{-5}	3.268×10^{-6}
3	0.2	1.25	3	1.27	92.72	1.072×10^{-5}	5.346×10^{-6}
4	0.2	1.25	5	1.54	116.30	9.795×10^{-6}	2.504×10^{-6}
5	0.4	0.80	1	6.18	410.53	5.207×10^{-6}	6.121×10^{-7}
6	0.4	1.00	0	4.34	143.37	6.371×10^{-6}	1.418×10^{-6}
7	0.4	1.25	5	1.55	67.04	7.487×10^{-6}	1.990×10^{-6}
8	0.4	1.25	3	1.68	81.85	9.500×10^{-6}	2.422×10^{-6}
9	0.6	0.80	3	9.12	540.20	3.893×10^{-6}	4.791×10^{-7}
10	0.6	1.00	5	2.78	199.02	4.141×10^{-6}	1.172×10^{-6}
11	0.6	1.25	0	0.91	53.19	8.535×10^{-6}	2.057×10^{-6}
12	0.6	1.25	1	1.52	81.34	7.470×10^{-6}	1.783×10^{-6}
13	0.2	0.80	5	4.33	191.20	5.956×10^{-6}	1.264×10^{-6}
14	0.2	1.00	3	1.73	89.69	9.880×10^{-6}	1.623×10^{-6}
15	0.2	1.25	1	1.18	59.29	1.600×10^{-5}	7.387×10^{-6}
16	0.2	1.25	0	0.87	51.22	1.755×10^{-5}	8.036×10^{-6}

3. Results

3.1. Rheological Analysis of Cement-Bentonite Slurry

In this section, the effect of water–cement ratio on the rheological properties of pure cement slurry is investigated first, followed by the analysis of the influence of bentonite content on the rheological characteristics of cement-bentonite slurry.

3.1.1. Effect of Water–Cement Ratio on Rheological Properties of Slurry

1. Rheological characteristics

The variation in the flow properties of the slurry during the permeation grouting process can be assessed through its rheological properties. However, during the preparation of pure cement slurry, the slurry undergoes hydration and crystallization, while during rheological measurements, stirring the slurry can lead to crystal destruction. This means that the rheological measurement is affected by both the hydration-crystallization process and crystal destruction [29], resulting in significant fluctuations in the rheological curves. Therefore, in this study, the rheological curves of slurry with 60 min standing time were selected for comparison.

Figure 6 presents the rheological curves of pure cement slurry at different water–cement ratios after 60 min of standing, along with the corresponding plastic viscosity and yield stress. As shown in Figure 6, the pure cement slurry with water–cement ratios of 0.80 and 1.00 exhibited distinct yield stress, and the shear stress showed a nearly linear relationship with the shear rate, which obeyed the Bingham fluid rheological characteristics. Notably, at a lower water–cement ratio (0.80), the slurry exhibited a higher yield stress. At a water–cement ratio of 1.25, the rheological curve approached a straight line passing through the origin, resembling a Newtonian fluid. As the water–cement ratio increased, both the plastic viscosity and yield stress of the pure cement slurry decreased.

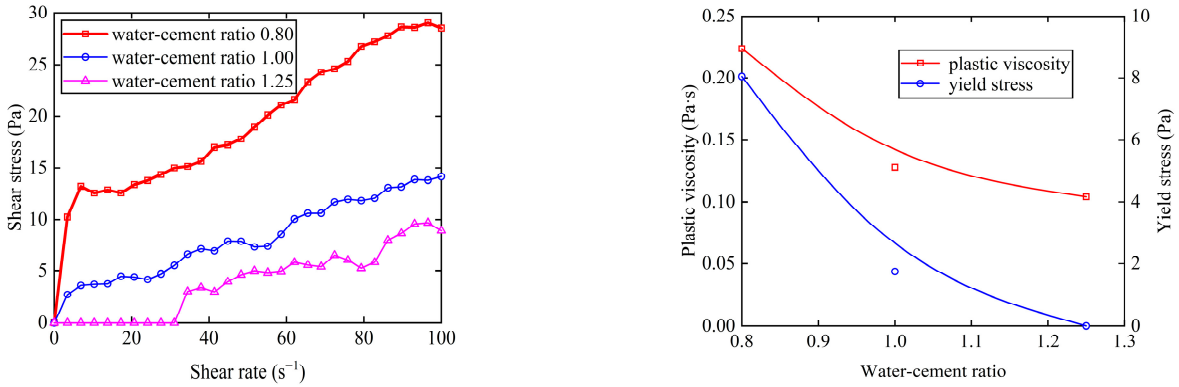

(**a**) (**b**)

Figure 6. Influence of water–cement ratio on rheological properties. (**a**) Rheological profiles at varying water–cement ratios, (**b**) Plastic viscosity and yield stress corresponding to each rheological profile.

2. Temporal variation of slurry viscosity and yield stress

Figure 7 illustrates the temporal variation of yield stress and plastic viscosity of pure cement slurry at water–cement ratios of 0.80, 1.00, and 1.25. As shown in Figure 7a, the appearance time of yield stress was progressively delayed as the water–cement ratio increased: at a water–cement ratio of 0.80, the yield stress was evident from beginning and stabilized after 15 min; at a ratio of 1.00, the yield stress appeared after 30 min and stabilized after 45 min; whereas at a ratio of 1.25, the yield stress was not observed even after 60 min. This delay can be attributed to the fact that the slurry gelation process can be divided into two stages [30]. In the first stage, the gelation is incomplete, and the slurry exhibits good flowability, resulting in lower shear stress that does not reach the lower limit of the rheometer measurement. In the second stage, the gelation is complete, and the slurry becomes more stable, with minimal variation in shear stress over time [31]. A higher water–cement ratio extends the time required for slurry to reach the stable phase, thereby delaying the manifestation of yield stress.

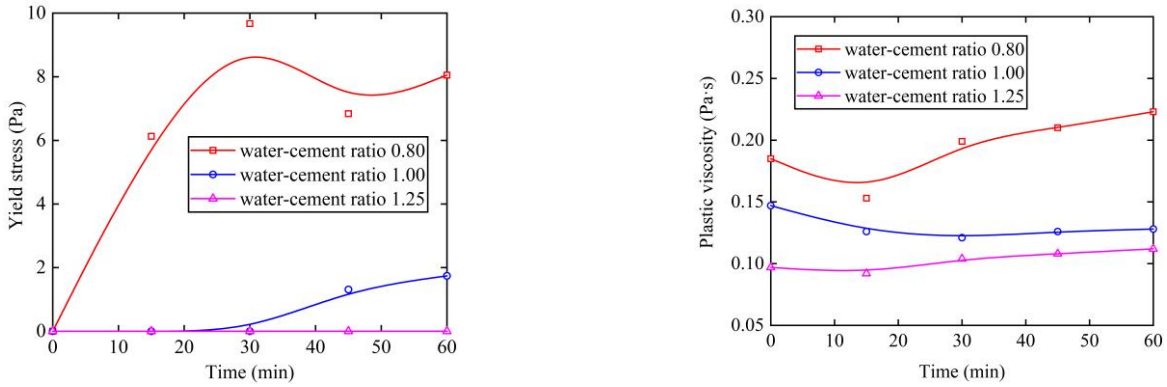

(**a**) Temporal variation curve of yield stress (**b**) Temporal variation curve of plastic viscosity

Figure 7. Influence of water–cement ratio on the time-dependent behavior of rheological properties.

The temporal variation of plastic viscosity for pure cement slurry with different water–cement ratios followed a similar pattern: decreased first and increased afterwards (Figure 7b). This was likely due to the instability of the slurry properties at the early stages of reaction, where rapid water separation leads to reduction in viscosity. As the water separation is completed and the slurry gradually gels, the viscosity increases over time [32].

3.1.2. Effect of Bentonite Content on the Rheological Properties of Slurry

1. Rheological characteristics

Figure 8 illustrates the influence of bentonite content on the rheological properties of cement-bentonite slurry. It can be seen from Figure 8a that the addition of bentonite did not alter the flow type of slurry, and all rheological curves conformed to the characteristics of Bingham fluids.

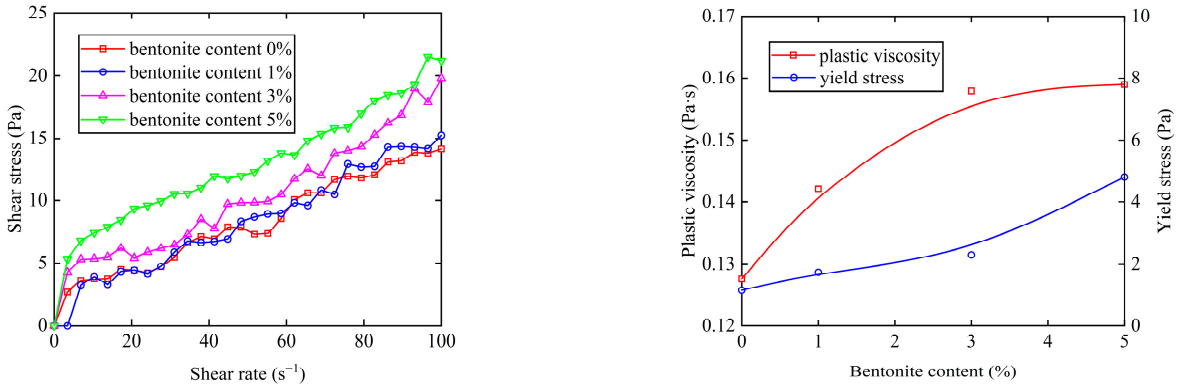

(**a**) (**b**)

Figure 8. Impact of bentonite content on rheological properties. (**a**) Rheological profiles at various bentonite contents, (**b**) Plastic viscosity and yield stress corresponding to various bentonite contents.

As shown in Figure 8b, the impact of bentonite on the plastic viscosity and yield stress of slurry was pronounced: as the bentonite content increased, both the yield stress and plastic viscosity of the cement-bentonite slurry increased progressively, with the trend of increasing plastic viscosity gradually decelerating. This can be explained by the following reasons: Firstly, bentonite, acting as an external additive, increased the solid particle content within the slurry, thereby raising the plastic viscosity and yield stress. Additionally, higher shear stress is needed to disrupt the initial crystalline structure due to the thixotropic properties of bentonite, especially at higher bentonite contents, thus increasing the yield stress of slurry. Furthermore, since bentonite exhibits shear-thinning behavior, its influence on the viscosity of cement-bentonite slurry diminished as the shear rate increased, leading to a gradual deceleration in the increment of plastic viscosity.

2. Temporal variation of slurry viscosity and yield stress

Figure 9 illustrates the temporal variation curves of plastic viscosity and yield stress for cement-bentonite slurries with a water–cement ratio of 0.80 and varying bentonite contents. As shown in Figure 9, for bentonite contents of 0% and 1%, the viscosity of slurry did not significantly change over time, as the hydration reaction of slurry concluded after 30 min, resulting in stable viscosity. At a bentonite content of 3%, the slurry viscosity initially decreased and then increased, while at a bentonite content of 5%, the viscosity increased exponentially over time, without a phase of decrease. The absence of decrease in viscosity indicates that the bleeding effect of slurry was no longer pronounced, suggesting that the addition of bentonite effectively mitigated the bleeding effect, enhancing the stability of slurry during the grouting process. Moreover, the continued change in viscosity beyond 30 min suggests that the hydration reaction was not yet complete, which indicates that the inclusion of bentonite slowed down the hydration process and improved the pumpability of slurry during grouting.

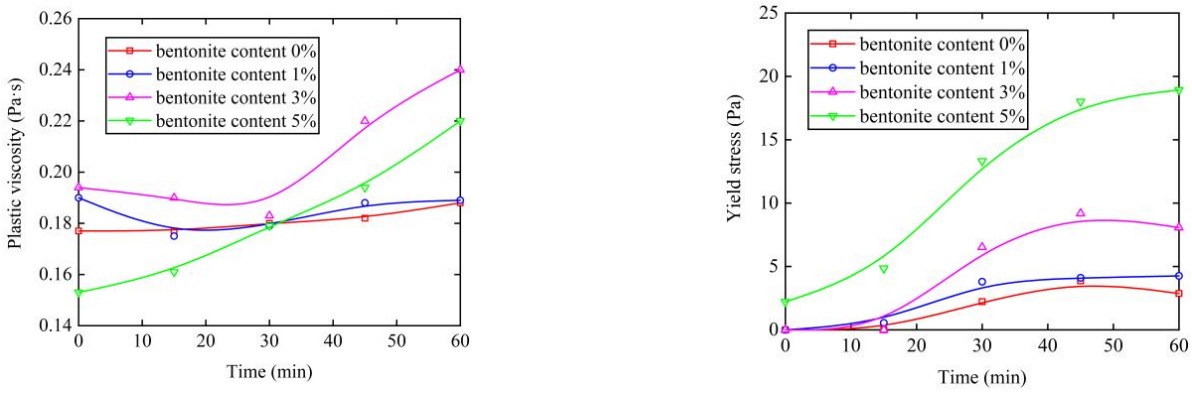

(**a**) Temporal variation curve of plastic viscosity (**b**) Temporal variation curve of yield stress

Figure 9. Influence of bentonite content on the time-dependent behavior of rheological properties.

For bentonite contents of 0% and 1%, the yield stress of slurry showed minimal change over time, making the temporal effect on yield stress negligible. However, as the bentonite content increased, the yield stress significantly rose over time, indicating a noticeable temporal effect. In practical grouting applications, a higher yield stress necessitates greater grouting pressure to achieve the desired grouting objectives. Therefore, the temporal changes in yield stress cannot be ignored for cement-bentonite slurry injection.

3.2. Analysis of Primary Controlling Factors for Seepage Prevention and Reinforcement

3.2.1. Analysis of Primary Controlling Factors for Compressive Strength

The maximum bearing capacity of the grouted body can be measured by its compressive strength. Before grouting, the injected medium consisted of loose sand particles, which were unable to reach a stable state, resulting in a bearing capacity of zero. After the completion of grouting, the sand particles were bonded by slurry and formed a stable structure, thereby enhancing the compressive strength. The experimental results are presented in Table 6. According to the compressive strength data in Table 6, the 3-day compressive strength of the specimens ranged from 0.5 to 9.5 MPa, indicating significant variability under different conditions.

Figure 10 illustrates the influence of grouting pressure, water–cement ratio, and bentonite content on the compressive strength of the grouted body. As shown in Figure 10, the compressive strength of the grouted body increased non-linearly with the increase in grouting pressure. At higher grouting pressures, more solid particles were injected into the pores of the grouted body, expelling water and resulting in a higher concentration of cementitious materials within the grouted body. This led to improved bonding properties of the grouted sample, thereby increasing the compressive strength of the grouted body. However, once the grouting pressure reached a certain level, further increases in pressure did not significantly enhance compressive strength.

The compressive strength of the grouted body decreased as the water–cement ratio increased (Figure 10). This phenomenon can be attributed to the higher water content in slurry with increased water–cement ratio. Since the amount of water required for the hydration reaction was fixed, the excess water remained within the sample, which reduced its bonding properties. Consequently, as the water–cement ratio rose, the compressive strength of the grouted body decreased.

The compressive strength of the grouted body first increased and then decreased as the bentonite content increased, indicating the existence of an optimal bentonite content (Figure 10). Adding an appropriate amount of bentonite to the slurry can improve the pore structure of the specimen, ensuring a uniform distribution of fine air bubbles in the

pores. This reduces the stress concentration under load, thereby enhancing the compressive strength of the grouted body [11]. However, at higher bentonite contents, excessive bentonite can significantly inhibit the hydration reaction of slurry, imparting a plasticizing effect on the grouted body, which reduces its compressive strength. Therefore, with increasing bentonite content, the compressive strength of the grouted body first increased and then decreased, with an optimal bentonite content at about 3%.

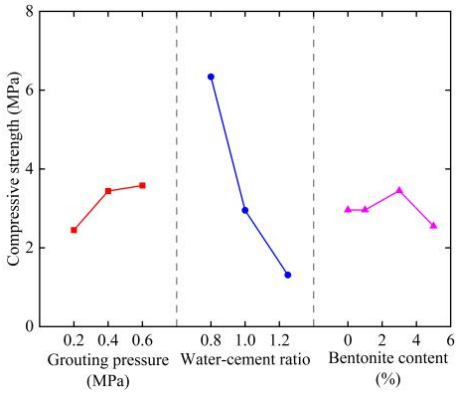

Figure 10. Influence of various factors on compressive strength.

Further, range analysis was performed to analyze the primary controlling factors that affected the compressive strength of the grouted body. The results are shown in Table 7.

Table 7. Results of compressive strength range.

Levels	Factor 1 Grouting Pressure (MPa)	Factor 2 Water–Cement Ratio (MPa)	Factor 3 Bentonite Content (MPa)
1	2.45	6.34	2.96
2	3.44	2.95	2.96
3	3.58	1.31	3.45
4	-	-	2.55
R	1.13	5.02	0.9

As listed in Table 7, it can be concluded that the sequence of influence of the three factors on the compressive strength of the grouted body was as follows: water–cement ratio > grouting pressure > bentonite content. Therefore, the water–cement ratio was the primary controlling factor for the compressive strength of the grouted body.

3.2.2. Analysis of Primary Controlling Factors for Deformation Modulus

The difficulty in deformation of the grouted body can be assessed by the deformation modulus. Prior to grouting, loose sand samples were unstable, resulting in a deformation modulus of zero. After grouting, the deformation modulus of the samples increased, as presented in Table 6. The deformation modulus data in Table 6 reveal that the deformation modulus of the grouted samples ranged from 50 to 550 MPa, showing significant variability under different conditions. The effects of various factors on the deformation modulus of the grouted sample are illustrated in Figure 11.

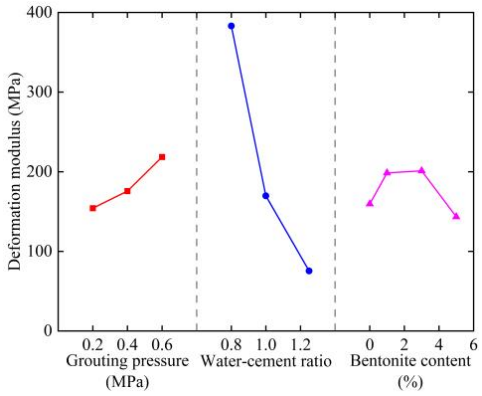

Figure 11. Influence of various factors on deformation modulus.

The deformation modulus of the grouted sample showed an increasing trend with higher grouting pressure. On the contrary, as the water–cement ratio increased, the deformation modulus exhibited a decreasing trend. With the addition of bentonite to the grout, the deformation modulus first increased and then decreased, with an optimal bentonite content of 3%. In general, the variation in the deformation modulus in response to these factors was consistent with that for compressive strength, indicating that during the cement hydration process, the compressive strength and the deformation modulus of the samples grew synchronously.

Through range analysis, it was determined that the influence of the three factors on the deformation modulus of the grouted mass was ranked as follows: water–cement ratio > grouting pressure > bentonite content. The water–cement ratio was identified as the primary controlling factor affecting the deformation modulus of the grouted body (Table 8).

Table 8. Results of the deformation modulus range.

Levels	Factor 1 Grouting Pressure (MPa)	Factor 2 Water–Cement Ratio (MPa)	Factor 3 Bentonite Content (MPa)
1	154.21	383.09	159.56
2	175.70	168.72	198.49
3	218.44	75.37	201.12
4	-	-	143.39
R	64.23	307.72	57.73

3.2.3. Analysis of Primary Controlling Factors for Permeability Coefficient

The impermeability of the grouted body can be assessed by the permeability coefficient. Prior to grouting, the permeability coefficient of the samples was about 2.54×10^{-1} cm/s. After grouting, the impermeability of the samples improved significantly: the permeability coefficient of the grouted sample was in the order of 10^{-5} to 10^{-6} cm/s after 6 h curing, and it further decreased to the order of 10^{-6} to 10^{-7} cm/s after 12 h curing, indicating an improvement of nearly one order of magnitude within 6 h.

Figure 12 illustrates the effects of grouting pressure, water–cement ratio, and bentonite content on the permeability coefficient of the grouted samples. As shown in Figure 12, the changing trends in permeability coefficient across different time intervals were consistent. With increasing grouting pressure, the permeability coefficient of the grouted samples decreased. Conversely, with an increasing water–cement ratio, the permeability coefficient of the grouted samples rose. The permeability coefficient decreased with an increase in bentonite content. When a higher grouting pressure was applied, more solid particles were

forced into the pores of the grouted body, filling the voids and expelling moisture, thereby reducing the porosity and permeability of the grouted body. Consequently, as grouting pressure increased, the impermeability of the grouted body improved. In contrast, a higher water–cement ratio caused excess water that remained within the specimen, increasing the porosity and permeability, thus reducing the impermeability. The impact of bentonite on the impermeability of the grouted body was significant. Bentonite, primarily composed of montmorillonite, is a hydrous silicate of aluminum. Upon contact with water, moisture molecules enter and fill the negatively charged interlayers of montmorillonite, causing the layers to expand. Bentonite particles either bind with cement or fill the structure of the grouted sample, resulting in a denser structure and thus reducing both porosity and permeability of the grouted samples [33]. Therefore, as the bentonite content increases, the impermeability of the grouted body improves.

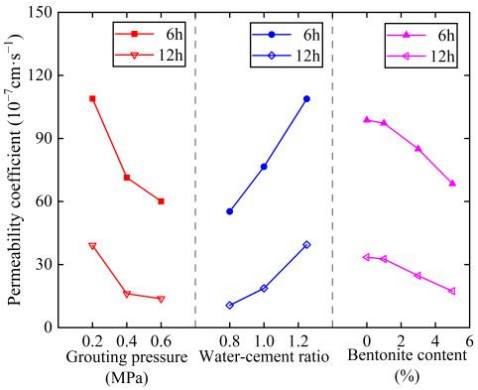

Figure 12. Influence of various factors on permeability.

Based on the findings shown in Table 9, the influence of grouting pressure, water–cement ratio, and bentonite content on the permeability coefficient of the grouted body after 6 h and 12 h curing was consistent. The order of their impact was as follows: water–cement ratio > grouting pressure > bentonite content. Thus, the water–cement ratio was determined to be the principal controlling factor affecting the permeability coefficient of the grouted body.

Table 9. Results of the permeability coefficient range.

Projects	Levels	Factor 1 Grouting Pressure (10^{-7} cm/s)	Factor 2 Water–Cement Ratio (10^{-7} cm/s)	Factor 3 Bentonite Content (10^{-7} cm/s)
6 h permeability coefficient	1	108.96	55.23	98.73
	2	71.41	76.55	97.27
	3	60.10	108.82	84.98
	4	-	-	68.45
	R1	48.86	53.59	30.29
12 h permeability coefficient	1	39.13	10.58	33.47
	2	16.11	18.70	32.63
	3	13.73	39.41	24.68
	4	-	-	17.32
	R2	25.40	28.83	16.14

In summary, the water–cement ratio was the primary controlling factor for the grouting reinforcement effectiveness. As the water–cement ratio increased, the compressive strength, deformation modulus, and impermeability of the grouted body decreased significantly. The impact of grouting pressure was secondary, showing a positive correlation with the compressive strength, deformation modulus, and impermeability of the grouted body. Bentonite content also played a crucial role in the grouting effectiveness: as the bentonite content increased, the compressive strength and deformation modulus of the grouted solid rose first and then decreased, indicating an optimal bentonite content level. Conversely, the impermeability of the grouted body improved with increased bentonite content.

3.3. Failure Characteristics of the Grouting Reinforcement Body

The failure characteristics of the grouted body reflect its overall integrity to some extent. Uniaxial compression tests on the grouted body revealed that the grouting pressure, water–cement ratio, and bentonite content significantly affected the failure characteristics (Figure 13).

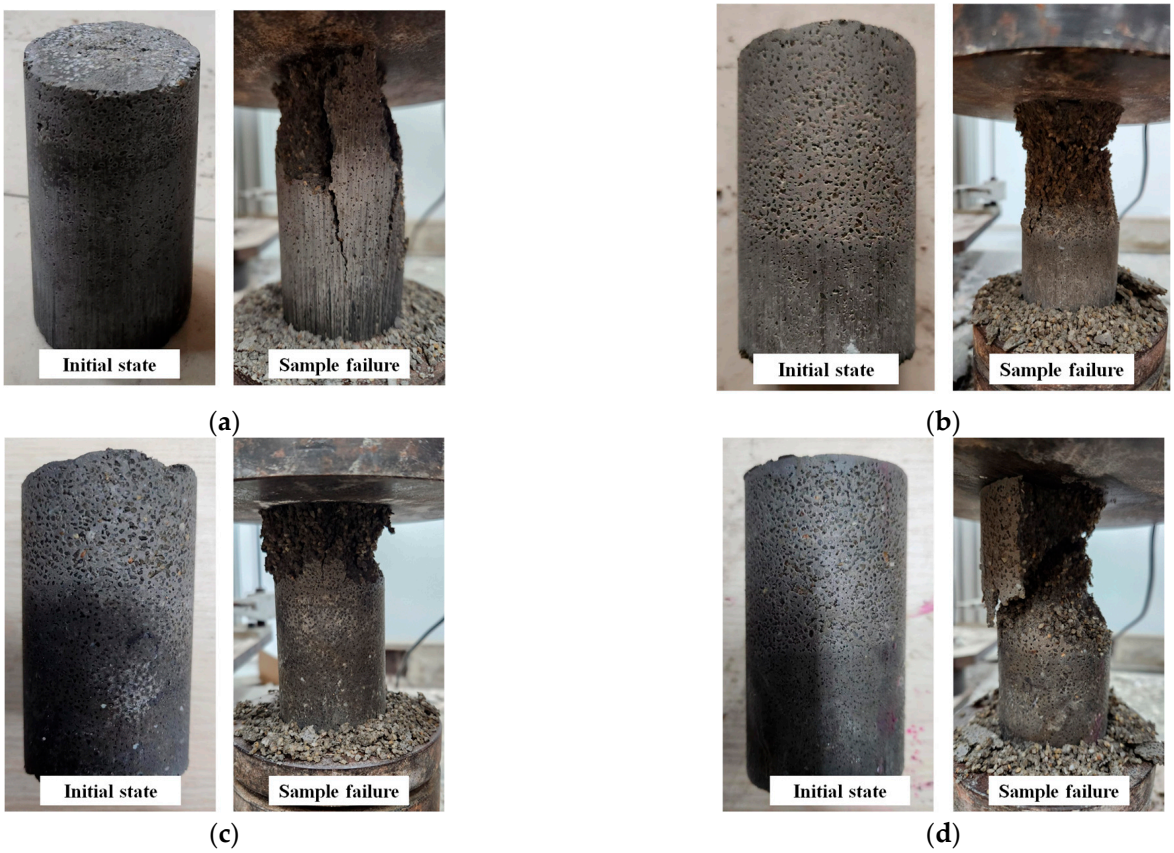

Figure 13. Failure characteristics of grouted soil. (**a**) Grouting pressure: 0.2 MPa, water–cement ratio: 0.80, bentonite content: 0%, (**b**) Grouting pressure: 0.2 MPa, water–cement ratio: 1.25, bentonite content: 3%, (**c**) Grouting pressure: 0.6 MPa, water–cement ratio: 1.25, bentonite content: 0%, (**d**) Grouting pressure: 0.2 MPa, water–cement ratio:1.25, bentonite content: 0%.

3.3.1. Impact of the Water–Cement Ratio

Figure 13a,d show the initial and failure states of samples with different water–cement ratios under the same grouting pressure (0.2 MPa) and bentonite content (0%). At a low water–cement ratio (Figure 13a), the initial state of the sample was relatively uniform and dense. Upon failure, several cracks traversed the entire grouted sample, indicating a characteristic of overall failure. In contrast, at a higher w/c ratio (Figure 13d), the initial state showed noticeable color variations, reflecting some degree of heterogeneity: the lower

part of the sample was darker and more compact, while the upper part was lighter in color, exhibiting a honeycomb structure with some exposed sand particles. During the uniaxial compression test, the sand particles in the upper part of the sample detached, while the lower part showed no significant change, demonstrating localized failure characteristics. This discrepancy may be attributed to the following reasons: at a low water–cement ratio, the grout injected into the sample did not suffer significant water separation effects [34], and the grout particles did not undergo substantial sedimentation, thus maintaining a uniform and dense grouted solid. In contrast, at a high water–cement ratio, water separation and sedimentation of particles in the grout occurred, leading to a more porous structure in the upper part of the grouted body and a denser structure in the lower part.

3.3.2. Impact of Grouting Pressure

Figure 13c,d display the initial and failure states of samples with the same water–cement ratio (1.25) and bentonite content (0%) under different grouting pressures. The initial state of the samples showed notable color differences between the upper and lower parts, indicating some degree of heterogeneity: the lower part was darker and more compact, while the upper part was lighter and more porous. Failure in all cases was characterized by localized damage, but the damage area was smaller when the grouting pressure was higher. At higher grouting pressure (Figure 13c), the volume of the compacted part of the sample was larger, while the volume of the porous part was smaller. In contrast, at lower grouting pressure (Figure 13d), the volume of the porous part of the sample was larger. This phenomenon can be explained by the following reasons: in both cases (water–cement ratio 1.25), there was a significant water separation effect after grout injection into the sample [34]. Cement particles moved from the upper part to the lower part of the sample due to the impact of gravity, resulting in particle sedimentation. The hydration reaction of the cement primarily occurred in the lower part of the sample, making the lower part of the grouted body denser and improving its mechanical properties. When the grouting pressure was higher, more grout particles were injected into the sample under the same conditions, and excess water was expelled, mitigating particle sedimentation and resulting in a larger volume of dense part of the grouted body and superior overall mechanical properties.

3.3.3. Impact of Bentonite Content

Figure 13b,d illustrate the initial and failure states of samples with the same water–cement ratio (1.25) and grouting pressure (0.2 MPa) but different bentonite contents. For bentonite contents of 0% and 3%, there was no significant difference in the initial and failure states of the samples—both initial states exhibited heterogeneity and localized failure under compression conditions.

Figure 14 presents the stress–strain curves for samples with different bentonite contents under the same water–cement ratio (1.25) and grouting pressure (0.2 MPa). It is evident that, for a bentonite content of 0%, the curve showed considerable fluctuations during the increase in stress, and the stress fluctuated with increasing strain after failure. In contrast, for the sample with bentonite content of 3%, the curve rose more smoothly, and the stress gradually decreased with increasing strain after failure. This can be attributed to the fact that the incorporation of bentonite improved the internal pore structure of the grouted body and resulted in a more uniform distribution of solid particles, thereby reducing the heterogeneity of the grouted body.

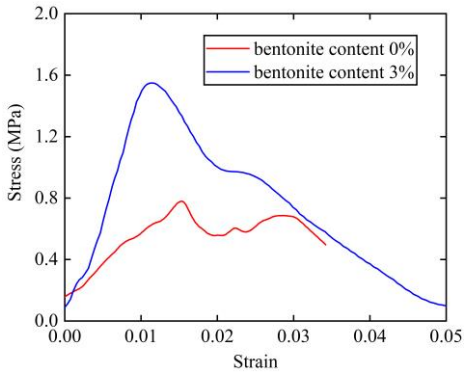

Figure 14. Stress–strain curves with various bentonite contents.

4. Conclusions

In this study, the rheological properties of cement-bentonite slurry and its performance in seepage control and reinforcement were investigated through a series of experiments. The following conclusions can be drawn:

The plastic viscosity and yield stress of the cement-bentonite slurry were positively correlated with the bentonite content. The temporal variation of plastic viscosity for slurries with different bentonite contents was complex: at low bentonite content, the plastic viscosity and yield stress exhibited minimal temporal variation; at moderate bentonite content, the plastic viscosity decreased first and then increased over time; at high bentonite content, both plastic viscosity and yield stress showed an increasing trend over time.

The water–cement ratio of the cement-bentonite slurry was the primary controlling factor for grouting reinforcement effect. As the water–cement ratio increased, the compressive strength, deformation modulus, and permeability coefficient of the grouted body significantly decreased. The impermeability of the grouted bodies was enhanced with increasing bentonite content. An increase in grouting pressure improved the grouting reinforcement effect. The compressive strength and deformation modulus of the grouted bodies increased first and then decreased with increasing bentonite content, and an optimal bentonite content can be identified.

As the water–cement ratio of the cement-bentonite slurry increased, the grouted bodies exhibited enhanced heterogeneity due to the water separation effect of the slurry, leading to a shift from overall to localized failure characteristics. An increase in grouting pressure and bentonite content helped to improve the pore structure of the grouted bodies and reduce heterogeneity.

The results of this work suggest that lower water–cement ratio is preferred for enhancing grouting reinforcement effect; moreover, the optimal bentonite content of the cement-bentonite slurry should be determined before engineering practice through experiments.

Author Contributions: Y.W.: formal analysis, supervision. T.Q.: data curation, investigation, writing—original draft. C.X.: investigation. J.G.: methodology, writing—review and editing. All authors have read and agreed to the published version of the manuscript.

Funding: This research was funded by the National Natural Science Foundation of China, grant number U2240210, 52279098, and the Fundamental Research Funds for the Central Universities, grant number B230201021.

Data Availability Statement: Data is contained within the article.

Conflicts of Interest: The authors declare no conflicts of interest.

References

1. Su, H.; Zhou, R. Research progress and prospect of earth-rockfill dam leakage detection modes and method. *Adv. Sci. Technol. Water Resour.* **2022**, *42*, 1–10. [CrossRef]
2. Zou, S. The Research on Theory and Application of the Flow-Fitting Method for Detection of Piping and Leakage in Dykes and Dams. Ph.D. Thesis, Central South University, Changsha, China, 2009.
3. Zhang, S. Research on the Groutability and Application of Permeation Grouting in Sand and Gravel Stratum. Ph.D. Thesis, Central South University, Changsha, China, 2007.
4. Kuang, J. *Theory and Project Example of Grout in Geotechnical Engineering*; Science Press: Beijing, China, 2001.
5. Li, S.; Sha, F.; Liu, R.; Zhang, Q.; Li, Z. Investigation on fundamental properties of microfine cement and cement-slag grouts. *Constr. Build. Mater.* **2017**, *153*, 965–974. [CrossRef]
6. Liu, J.; Wang, R.; Meng, Q.; Chen, L.; Wang, J.; Liu, J. Research progress on production technology, properties and engineering application of superfine cement. *Bull. Chin. Ceram. Soc.* **2023**, *42*, 1519–1528.
7. Carreño-Gallardo, C.; Tejeda-Ochoa, A.; Perez-Ordonez, O.; Ledezma-Sillas, J.; Lardizabal-Gutierrez, D.; Prieto-Gomez, C.; Valenzuela-Grado, J.; Robles Hernandez, F.; Herrera-Ramirez, J. In the CO_2 emission remediation by means of alternative geopolymers as substitutes for cements. *J. Environ. Chem. Eng.* **2018**, *6*, 4878–4884. [CrossRef]
8. Huang, W. Properties of cement-fly ash grout admixed with bentonite, silica fume, or organic fiber. *Cem. Concr. Res.* **1997**, *27*, 395–406. [CrossRef]
9. Mirza, J.; Riaz, M.; Naseer, A.; Rehman, F.; Khan, A.; Ali, Q. Pakistani bentonite in mortars and concrete as low cost construction material. *Appl. Clay Sci.* **2009**, *45*, 220–226. [CrossRef]
10. Jiang, L.; Wang, T.; Ding, G.; Chu, H.; Hu, J.; Na, B.; Xiong, C. Researches on performances and mechanism of bentonite-cement mortar. *New Build. Mater.* **2012**, *39*, 48–53. [CrossRef]
11. Li, S. Experimental Study on Filling Characteristics of Bentonite. Ph.D. Thesis, Jiangxi University of Science and Technology, Ganzhou, China, 2018.
12. Xu, W.; Rao, Y.; Li, S.; Xu, W. Analysis on bleeding performance of filling slurry with bentonite. *Gold Sci. Technol.* **2019**, *27*, 433–439. [CrossRef]
13. Todaro, C.; Saltarin, S.; Cardu, M. Bentonite in two-component grout applications. *Case Stud. Constr. Mater.* **2022**, *16*, e00901. [CrossRef]
14. Zhang, J.; Liang, W.; Han, J.; Han, X.; Yu, Y. Study on physical and mechanical characteristics of paste filling material with swelling properties. *Min. Res. Dev.* **2015**, *35*, 15–20. [CrossRef]
15. Zhao, N.; Wang, S.; Quan, X.; Wang, C. Study on the coupled effects of bentonite and high-volume fly ash on mechanical properties and microstructure of engineered cementitious composites (ECC). *KSCE J. Civ. Eng.* **2019**, *23*, 2628–2635. [CrossRef]
16. Wang, Q.; Wang, H.; Min, F. Effect of raw material ratio on properties of foam paste backfilling materials. *Mater. Rep.* **2015**, *29*, 135–139. [CrossRef]
17. Isaia, G.; Gastaldini, A.; Moraes, R. Physical and pozzolanic action of mineral additions on the mechanical strength of high-performance concrete. *Cem. Concr. Compos.* **2003**, *25*, 69–76. [CrossRef]
18. Santhoshkumar, T.; Abraham, B.; Sridharan, A.; Jose, B. Role of bentonite in improving the efficiency of cement grouting in coarse sand. *Geotech. Eng. J. SEAGS AGSSEA* **2016**, *47*, 136–143. [CrossRef]
19. Qing, P.; Fu, P. An Experimental Comparative Study of Stability Slurry in Sand and Gravel Layer Grouting. *Chin. Rural. Water Hydropower* **2014**, *5*, 111–114+117.
20. Cheng, W.; Ni, J.; Shen, J.; Wang, Z. Modeling of Permeation and Fracturing Grouting in Sand: Laboratory Investigations. *J. Test. Eval.* **2018**, *46*, 2067–2082. [CrossRef]
21. Zhang, J. Comparative experimental study on grouting of Stability Slurry in sandy gravel soil. *J. Hydraul. Eng.* **1993**, *7*, 69–74.
22. Chen, H. A Brief Discussion on the Application of Bentonite-Cement Grout in Curtain Grouting Projects in Fine Fracture Formations. *Water Resour. Dev. Manag.* **2011**, *31*, 17–20+16.
23. Li, Z.; Zhang, L.; Zhang, Q.; Liu, R.; Yang, W.; Chu, Y. Simulation test for permeation grouting reinforcement effect of sand layer. *J. China Coal Soc.* **2018**, *43*, 3488–3497. [CrossRef]
24. Wang, Q.; Zhu, Y.; Li, W.; Cui, P.; Pan, Y. Study on the mechanism of column permeation grouting of Bingham fluid considering the spatial attenuation of viscosity. *Chin. J. Rock Mech. Eng.* **2022**, *41*, 1647–1658. [CrossRef]
25. *GB/T50123-2019*; Standard of Geotechnical Test Method. China Planning Press: Beijing, China, 2019.
26. Huang, D.; Wang, Z.; Yang, B. *Formation Water Plugging and Reinforcement Construction Technology of Grouting*; China Mining University Press: Xuzhou, China, 2003.
27. Liu, Y.; Su, Y.; Yin, Y.; Zhao, J.; Wang, S.; Mo, Z. Research progress of bentonite modified cementitious materials. *Mater. Rep.* **2021**, *35*, 5040–5052. [CrossRef]
28. Zhang, C. *Experiment Design and Data Processing*; Chemical Industry Press: Beijing, China, 2009.
29. Xia, C.; Feng, X. Rheological test and research on stable cement paste. *Water Resour. Hydropower Eng.* **2004**, *35*, 78–81. [CrossRef]

30. Chu, Y. Mechanism Study on Fracture Grouting Based on Flow-Solid Phase Transformation Characteristics of Quick-Setting Cement. Ph.D. Thesis, China University of Petroleum, Dongying, China, 2024.
31. Ruan, W. Research on diffusion of grouting and basic properties of grouts. *Chin. J. Geotech. Eng.* **2005**, *27*, 69–73. [CrossRef]
32. Liu, J.; Zhang, G.; Yang, D.; Zhong, P. Rheological properties of clay-cement grouting material and influence on grouting. *Bull. Chin. Ceram. Soc.* **2016**, *35*, 2581–2589.
33. Xu, C.; Huang, L.; Xing, H. Influence of cement-bentonite slurry mixing ratio on permeability of cutoff wall. *Rock Soil Mech.* **2010**, *31*, 422–426. [CrossRef]
34. Li, X.; Zhang, Q.; Zhang, X.; Zuo, J.; Lan, X.; Yang, T. Research on water-bleeding property of cement slurry. *J. Build. Mater.* **2018**, *21*, 8–14. [CrossRef]

Disclaimer/Publisher's Note: The statements, opinions and data contained in all publications are solely those of the individual author(s) and contributor(s) and not of MDPI and/or the editor(s). MDPI and/or the editor(s) disclaim responsibility for any injury to people or property resulting from any ideas, methods, instructions or products referred to in the content.